Songklanakarin J. Sci. Technol.
45 (4), 483–493, Jul. – Aug. 2023

http://www.sjst.psu.ac.th

Original Article

Impact of radiation on MHD flow with hall effect and induced magnetic field over magnetized vertical surface

Arjun Agrawal and J. P. Panda*

Department of Mathematics, Veer Surendra Sai University of Technology, Burla, Odisha, India

Received: 28 July 2022; Revised: 14 November 2022; Accepted: 12 June 2023

Abstract

We investigate the impact of radiation parameter on MHD flow of a viscoelastic fluid over a vertical surface. The Hall effect and induced magnetic field (i.m.f) are applied. The model equations are solved analytically. The nature of pertinent parameters affecting velocity, i.m.f, temperature and concentration are analyzed. The novelty of the research is in investigating the impacts of radiation effect and i.m.f along with Hall current on the flow field. Important findings are: with the rise in thermal radiation, i.m.f falls in primary flow direction, whereas the reverse trend is noticed for secondary flow direction. We also found that radiation effect increases the fluid temperature and both the components of velocity profiles. The expressions of skin friction, current density, Nusselt and Sherwood number over the magnetized vertical surface (m.v.s) are computed and assessed graphically. It is also found that as the Nusselt number rises, skin friction on primary flow accelerates to maximum value then decelerates and current density on secondary flow accelerates with rise in the thermal radiation, whereas skin friction on secondary flow and current density on primary flow decelerate with increase in thermal radiation.

Keywords: viscoelastic fluid, radiation effect, MHD flow, Hall current, induced magnetic field (i.m.f)

1. Introduction

Magnetohydrodynamics, MHD, is the study of influence of magnetic field on electrically conducting fluids. MHD has many applications in biomedical engineering, such as magneto fluid rotary blood pumps, MRI, hyper thermic regulation, MHD pumps, bearings and boundary layer control. MHD waves and oscillations are useful to remote diagnostics. In the presence of a transverse magnetic field, the problem of hydro-magnetic behavior of the boundary layer along a static surface is of utmost importance. MHD boundary layer is relevant in many industrial systems retaining liquid metals and plasma flows transverse to a magnetic field. To study the MHD in the context of various flow situations, many efforts have been made, including Baitharu, Sahoo, and Dash (2021a, 2021b), Hayat, Abbas, and Sajid (2009), Hayat, Ullah, Muhammad, and Alsaedi (2017), Jamil, Khan, and Shahid (2013), Krishna (2021a), Krishna and Chamkha (2020), Osalusi, Side, Harris, and Clark (2008), Panigrahi, Kumar, and Panda (2021), Meher and Patel (2019, 2020) Panda, Dash, and Dash (2012), Sahoo, Panda, and Dash (2013), Singh, Shanker Seth, Vishwanath, and Rohidas (2020), Veera and Krishna (2020), Verma and Meher (2022).

The i.m.f affects the rate of flow and flow configuration, in ways that must be precisely regulated. I.m.f plays an important role in MHD flow due to several important contexts such as cosmic rays, sunspots, and plasma. Due to the applications in different scientific and technological phenomena, i.m.f has attracted several researchers. There are many studies where the i.m.f. has not been considered yet. Only a few researchers have considered the influence of i.m.f on boundary layer flows, such as Iqbal *et al.*, 2020; Iqbal, Maraj, Azhar, and Mehmood, 2017; Koshiba, Mutsushita, and Ishikawa, 2002.

Thermal radiation has several uses in biomedical fields because of its application in medical treatment. The results of thermal radiation with double diffusion have become a significant research topic. Infrared radiation is widely applicable in heat treatments of various parts of the body. Infrared radiation is electromagnetic waves between microwaves and visible light. It is useful in curing many skin-related disorders. The parameters pigmentation, vascularity,

*Corresponding author
Email address: jppanda_math@vssut.ac.in

and wavelength of radiation are determinants of the radiation entering the skin. The radiative effect has significant applications in space technology and in high temperature processes. Thermal radiation is also significant in nuclear power plants, gas turbines, and the various propulsion devices of aircraft, missiles, satellites and space vehicles. The radiation heat transfer effects on different flows are vital Baitharu, Sahoo, and Dash (2020a, 2020b), Chaudhary, Sharma, and Jha (2006), Khemissat, Bouaziz, and Bouaziz (2022), Krishna (2021b), Pandya and Quraishi (2018), Panigrahi, Kumar, and Panda (2021), Sahoo, Rout, and Dash (2022), VeeraKrishna, Subba Reddy, and Chamkha (2018).

Motivated by the above studies, the novelty of our work is that we have analyzed the radiation effect on MHD mixed convection flow over magnetized vertical surface with Hall current and induced magnetic field. Our work has many applications in nature as well as in engineering, such as in photosynthetic mechanism, calm day evaporation, vaporization of fog and mist, chemical vapor deposition, cooling of electronic equipment, and so forth. We have extended the research of Singh *et al.* (2020) by applying radiation effect. We have used the perturbation technique to solve the governing equations. The nature of pertinent parameters such as radiation parameter, Schmidt number, Hall parameter, etc., with velocity, i.m.f, temperature and concentration, is investigated graphically. Also, the behavior of different physical parameters on the fluid surface such as skin friction, current density, Nusselt number and Sherwood number are computed and represented in figures.

2. Problem Formulation

We presume steady laminar flow of a viscoelastic, incompressible, and electrically conducting fluid over a magnetized vertical porous surface. The flow of the fluid is affected by the strong magnetic field h_0 parallel to y'-axis and rotating flow along y'-axis is applied with angular velocity $\vec{\Omega}$. The vertical surface is normal to y'-axis and coincides with xz'- plane. We have considered the m.v.s to be porous which allows fluid to flow across it with transportation velocity $-v_0$. Due to buoyancy the fluid flow is induced. Magnetic diffusivity of fluid is assumed to be negligible in the study of i.m.f. The physical model problem is presented in Figure 1. The model equations (Singh, Shanker Seth, Vishwanath, & Rohidas, 2020) are as follows.

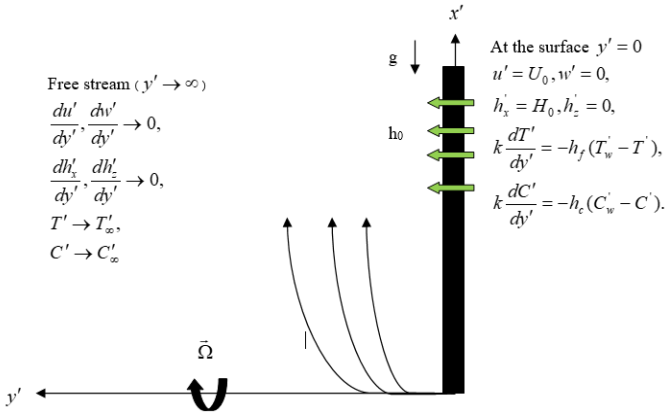

Figure 1. Flow geometry of the model

Momentum equations (Singh, Shanker Seth, Vishwanath, & Rohidas, 2020):

$$2\Omega w' - v_0 \frac{du'}{dy'} = v_e \frac{d^2u'}{dy'^2} + \frac{\mu_e h_0}{\rho}\frac{dh'_x}{dy'} - \frac{\beta' v_0}{\rho}\frac{d^3u'}{dy'^3} - \frac{v_f u'}{k'} + g\beta_T(T' - T'_\infty) + g\beta_C(C' - C'_\infty), \tag{1}$$

$$-2\Omega u' - v_0 \frac{dw'}{dy'} = v_e \frac{d^2w'}{dy'^2} + \frac{\mu_e h_0}{\rho}\frac{dh'_z}{dy'} - \frac{\beta' v_0}{\rho}\frac{d^3w'}{dy'^3} - \frac{v_f w'}{k'}. \tag{2}$$

Magnetic induction equations (Singh, Shanker Seth, Vishwanath, & Rohidas, 2020):

$$-\frac{d^2h'_x}{dy'^2} + m\frac{d^2h'_z}{dy'^2} = \sigma\mu_e h_0 \frac{du'}{dy'} + \sigma\mu_e v_0 \frac{dh'_x}{dy'}, \tag{3}$$

$$-\frac{d^2h'_z}{dy'^2} - m\frac{d^2h'_x}{dy'^2} = \sigma\mu_e h_0 \frac{dw'}{dy'} + \sigma\mu_e v_0 \frac{dh'_z}{dy'}. \tag{4}$$

Energy equation (Singh, Shanker Seth, Vishwanath, & Rohidas, 2020):

$$-v_0 \frac{dT'}{dy'} = \frac{k}{\rho C_p}\frac{d^2T'}{dy'^2} - \frac{S^*}{\rho C_p}(T' - T'_\infty) - \frac{1}{\rho C_p}\frac{dq_r}{dy'}. \tag{5}$$

Concentration equation (Singh, Shanker Seth, Vishwanath, & Rohidas, 2020):

$$-v_0 \frac{dC'}{dy'} = D\frac{d^2C'}{dy'^2} - K'(C' - C'_\infty). \tag{6}$$

Boundary conditions (b.c.) (Singh, Shanker Seth, Vishwanath, & Rohidas, 2020):

$$u'=U_0, w'=0, h'_x=H_0, h'_z=0, k\frac{dT'}{dy'}=-h_f(T'_w-T'), D\frac{dC'}{dy'}=-h_c(C'_w-C'), at\ y'=0,$$
$$\frac{du'}{dy'}, \frac{dw'}{dy'}, \frac{dh'_x}{dy'}, \frac{dh'_z}{dy'} \to 0, T'\to T'_\infty, C'\to C'_\infty \qquad as\ y'\to\infty \tag{7}$$

Applying Rosseland approximation (Krishna (2021)):

$$q_r=\frac{-4\sigma'}{3k'}\frac{dT'^4}{dy'}, \tag{8}$$

where σ'= "Stefan- Boltzmann constant", k'="mean absorption coefficient",

$$T'^4\cong 4T'^3_\infty T'-3T'^4_\infty. \tag{9}$$

On using equation (9) in equation (8), we get,

$$q_r=\frac{-16\sigma' T'^3_\infty}{3k'}\frac{dT'}{dy'}. \tag{10}$$

On using equation (10) in equation (5), we get,

$$-v_0\frac{dT'}{dy'}=\frac{k}{\rho C_p}\frac{d^2T'}{dy'^2}-\frac{S^*}{\rho C_p}(T'-T'_\infty)+\frac{1}{\rho C_p}\frac{16\sigma' T'^3_\infty}{3k'}\frac{d^2T'}{dy'^2}. \tag{11}$$

Using $q'=u'+iw'$ and $h'=h'_x+ih'_z$, in equation (1) to equation (4) and merging them gives

$$-2i\Omega q'-v_0\frac{dq'}{dy'}=v_e\frac{d^2q'}{dy'^2}+\frac{\mu_e h_0}{\rho}\frac{dh'}{dy'}-\frac{\beta' v_0}{\rho}\frac{d^3q'}{dy'^3}-\frac{v_f q'}{k'}+g\beta_T(T'-T'_\infty)+g\beta_C(C'-C'_\infty), \tag{12}$$

$$-(1+im)\frac{d^2h'}{dy'^2}=\sigma\mu_e h_0\frac{dq'}{dy'}+\sigma\mu_e v_0\frac{dh'}{dy'}, \tag{13}$$

B. c. in equation (7) in compact form is

$$q'=U_0, h'=H_0, k\frac{dT'}{dy'}=-h_f(T'_w-T'), D\frac{dC'}{dy'}=-h_c(C'_w-C'), \qquad at\ y=0,$$
$$\frac{dq'}{dy'}, \frac{dh'}{dy'}\to 0, T'\to T'_\infty, C'\to C'_\infty, \qquad as\ y\to\infty \tag{14}$$

Using following dimensionless quantities

$$y=\frac{U_0 y'}{v_e}, q=\frac{q'}{U_0}, h=\frac{h'}{U_0}\sqrt{\frac{\mu_e}{\rho}}, T=\frac{T'-T'_\infty}{T'_w-T'_\infty}, C=\frac{C'-C'_\infty}{C'_w-C'_\infty}. \tag{15}$$

in equation (6), equation (11), equation (12) and equation (13), we obtain the dimensionless equations

$$(1+N)\frac{d^2T}{dy^2}+SP_r\frac{dT}{dy}-\phi P_r T=0, \tag{16}$$

$$\frac{d^2C}{dy^2}+SS_c\frac{dC}{dy}-K_1S_cC=0, \tag{17}$$

$$S\beta\frac{d^3q}{dy^3}-S\frac{dq}{dy}=\frac{d^2q}{dy^2}+M\frac{dh}{dy}+E_1q+G_TT+G_CC, \tag{18}$$

$$-(1+im)\frac{d^2h}{dy^2}=MP_m\frac{dq}{dy}+SP_m\frac{dh}{dy}, \tag{19}$$

where,

$$S=\frac{v_0}{U_0}, \Pr=\frac{v_e\rho C_p}{k}, \phi=\frac{S^*v_e}{\rho C_p U_0^2}, Sc=\frac{v_e}{D}, K_1=\frac{K'v_e}{U_0^2}, M=\frac{h_0}{U_0}\sqrt{\frac{\mu_e}{\rho}}, E=\frac{\Omega v_e}{U_0^2}, N=\frac{16\sigma' T'^3_\infty}{3kk'},$$
$$\beta=\frac{\beta' U_0^2}{\rho v_e^2}, K=\frac{k'U_0^2}{v_e v_f}, G_T=\frac{g\beta_T(T'_w-T'_\infty)v_e}{U_0^3}, G_C=\frac{g\beta_C(C'_w-C'_\infty)v_e}{U_0^3}, v_m=\frac{1}{\sigma\mu_e}, E_1=2iE-\frac{1}{K}, Pm=\frac{v_e}{v_m}.$$

The b.c.in equation (14) is converted to

$$q=1, h=M_0, \frac{dC}{dy}=F_i(C-1), \frac{dT}{dy}=B_i(T-1), at\ y=0,$$
$$\frac{dh}{dy}, \frac{dq}{dy}, C, T\to 0, \qquad at\ y\to\infty. \tag{20}$$

where,

$$M_0 = \frac{H_0}{U_0}\sqrt{\frac{\mu_e}{\rho}}, B_i = \frac{\nu_e h_f}{kU_0}, F_i = \frac{\nu_e h_c}{DU_0}.$$

3. Solutions

The solution of equation (16) and equation (17) with the b.c. in equation (20) is as follows.

Fluid temperature (T)

$$T = Ae^{-m_1 y}, \tag{21}$$

where,

$$m_1 = \frac{\frac{SP_r}{1+N} + \sqrt{\left(\frac{SP_r}{1+N}\right)^2 + 4\left(\frac{\phi P_r}{1+N}\right)}}{2}, \tag{22}$$

$$A = \frac{B_i}{m_1 + B_i}. \tag{23}$$

Fluid concentration $C = Be^{-n_1 y}$, (24)

where,

$$n_1 = \frac{SS_c + \sqrt{(SS_c)^2 + 4K_1 S_c}}{2}, \tag{25}$$

$$B = \frac{F_i}{F_i + n_1}, \tag{26}$$

A regular perturbation method is applied to solve equation (18) and equation (19). We considered perturbations of the fluid velocity (q) and the i.m.f (h) as follows:

$$q = q_{00} + Sq_{01} + O(S^2), \tag{27}$$

and

$$h = h_{00} + Sh_{01} + O(S^2), \tag{28}$$

where S is a very small value.

Putting equation (27) and equation (28) in equation (18) and equation (19) gives 0th and 1st order perturbation equations, which are as follows.

0th-order equations are

$$\frac{d^2 q_{00}}{dy^2} + M\frac{dh_{00}}{dy} + E_1 q_{00} = -G_T T - G_C C, \tag{29}$$

$$\frac{d^2 h_{00}}{dy^2} + \frac{MP_m}{1+im}\frac{dq_{00}}{dy} = 0. \tag{30}$$

1st-order equations are

$$\frac{d^2 q_{00}}{dy^2} + M\frac{dh_{00}}{dy} + E_1 q_{00} = \beta\frac{d^3 q_{00}}{dy^3} - \frac{dq_{00}}{dy}, \tag{31}$$

$$\frac{d^2 h_{01}}{dy^2} + \frac{MP_m}{1+im}\frac{dq_{01}}{dy} = -\frac{P_m}{1+im}\frac{dh_{01}}{dy}. \tag{32}$$

Putting equation (27) and (28) in b. c. for q and h in equation (20) gives these 0th and 1st order conditions.

0th-order b.c. is

$$\begin{aligned} &h_{00} = M_0, q_{00} = 1, at\ y = 0, \\ &\frac{dh_{00}}{dy}, \frac{dq_{00}}{dy} \to 0, at\ y \to \infty. \end{aligned} \tag{33}$$

1st-order b. c.is

$$\begin{aligned} &h_{01} = 0, q_{01} = 0, at\ y = 0, \\ &\frac{dh_{01}}{dy}, \frac{dq_{01}}{dy} \to 0, at\ y \to \infty. \end{aligned} \tag{34}$$

Solutions of 0th order perturbation equation (29) and (30) using 0th order b.c. in equation (33) yields

$$q_{00} = (1 + a_3 + a_4)e^{-l_1 y} - a_3 e^{-m_1 y} - a_4 e^{-n_1 y}, \tag{35}$$

$$h_{00} = \frac{1}{M}\left[MM_0 - (a_7 - a_5 - a_6) - a_5 e^{-m_1 y} - a_6 e^{-n_1 y} + a_7 e^{-l_1 y}\right], \tag{36}$$

where,

$$a_1 = G_T A, a_2 = G_C B, a_3 = \frac{a_1}{m_1^2 - l_1^2}, a_4 = \frac{a_2}{n_1^2 - l_1^2}, a_5 = \frac{(m_1^2 + E_1)a_3 - a_1}{m_1}, a_6 = \frac{(n_1^2 + E_1)a_4 - a_2}{n_1},$$

$$a_7 = \frac{(l_1^2 + E_1)(1 + a_3 + a_4)}{m_1}.$$

Solutions of 1st-order perturbation equation (31) and equation (32) using 1st order b.c. in equation (34) yields

$$q_{01} = (ya_8 - a_9 - a_{110})e^{-l_1 y} + a_9 e^{-m_1 y} + a_{10} e^{-n_1 y}, \tag{37}$$

$$h_{01} = \frac{1}{M}\left[(a_{12} + a_{13} + a_{14}) + (ya_{11} - a_{12})e^{-l_1 y} - a_{13} e^{-m_1 y} - a_{14} e^{-n_1 y}\right], \tag{38}$$

where,

$$a_8 = \frac{(1 + a_3 + a_4)l_1(\beta l_1^2 - 1) - \frac{P_m a_7}{1 + im}}{2l_1}, a_9 = \frac{m_1^2(\beta m_1^2 - 1)a_3 - \frac{P_m a_5 m_1}{1 + im}}{m_1(m_1^2 - l_1^2)}, a_{10} = \frac{n_1^2(\beta n_1^2 - 1)a_4 - \frac{P_m a_6 n_1}{1 + im}}{n_1(n_1^2 - l_1^2)},$$

$$a_{11} = \frac{a_8(l_1^2 + E_1)}{l_1}, a_{12} = \frac{a_8(l_1^2 - E_1)}{l_1^2} - (1 + a_3 + a_4)(\beta l_1^2 - 1) + (l_1 + \frac{E_1}{l_1})(a_9 + a_{10}),$$

$$a_{13} = \frac{m_1(\beta m_1^2 - 1)a_3 - (m_1^2 + E_1)a_9}{m_1}, \; a_{14} = \frac{n_1(\beta n_1^2 - 1)a_4 - (n_1^2 + E_1)a_{10}}{n_1}.$$

Putting the values of equation (35) and equation (37) in equation (27), we get q as follows,

$$q = [(1 + Sya_8) + (a_3 - Sa_9) + (a_4 - Sa_{10})]e^{-l_1 y} - (a_3 - Sa_9)e^{-m_1 y} - (a_4 - Sa_{10})e^{-n_1 y}. \tag{39}$$

Putting the values of equation (36) and equation (38) in equation (28), we get h as follows,

$$h = M_0 - \frac{1}{M}\{[(a_7 - Sa_{12}) - (a_5 - Sa_{13}) - (a_6 + Sa_{14})] - (a_7 + Sya_{11} - Sa_{12})e^{-l_1 y} \tag{40}$$

$$+ (a_6 + Sa_{14})e^{-n_1 y} + (a_5 + Sa_{13})e^{-m_1 y}\}.$$

4. Nusselt Number, Sherwood Number, Skin Friction and Current Density

Rate of heat transfer (Nu) at m.v.s is expressed as Nusselt number given by

$$Nu = -\left[\frac{dT}{dy}\right] = Am_1. \tag{41}$$

Rate of mass transfer (Sh) at the m.v.s is expressed as Sherwood number given by

$$Sh = -\left[\frac{dC}{dy}\right] = Bn_1. \tag{42}$$

Current density (J) at m.v.s in the primary and secondary flows directions is

$$J = J_x + iJ_z = -i\left[\frac{dh}{dy}\right]_{y=0} = -\frac{i}{M}\{Sa_{11} - l_1(a_7 - Sa_{12}) + n_1(a_6 + Sa_{14}) \tag{43}$$

$$+ m_1(a_5 + Sa_{13})\}.$$

Skin friction (τ) at m.v.s along the primary and secondary flows directions is

$$\tau = \tau_x + i\tau_z = \left[\frac{dq}{dy} - \beta S\frac{d^2 q}{dy^2}\right]_{y=0} = \{Sa_8(1 + 2\beta S l_1) - l_1(1 + l_1\beta S)\} + \tag{44}$$

$$\{(a_3 - Sa_9)(m_1 - l_1)[1 + \beta S(m_1 + l_1)] + \{(a_4 - Sa_{10})(n_1 - l_1)[1 + \beta S(n_1 + l_1)]\}.$$

5. Results and Discussion

Numerical computations have been run to study the impact of flow characteristics corresponding to different flow inducing parameters. Numerical results for velocity profile (q), i.m.f. (h), temperature profile (T) and concentration profile (C) are depicted graphically, and the numerical results for skin friction (τ), current density (J), Nusselt number (Nu) and Sherwood number (Sh) at the m.v.s are also assessed graphically. The flow inducing parameters held fixed were m=0.5, E=0.5, M=4, K=0.3, P_m=0.75, β=0.5, G_T=4, G_C=5, S=0.25, B_i=0.5, F_i=0.5, M_0=1, N=1, P_r=0.75, S_c=0.78, ϕ=1, K_1=0.2 during numerical computations.

5.1 Velocity field

Effects of various parameters were computed and are plotted for velocity field (q), i.m.f (h), temperature field (T) and concentration field (C). Figures 2, 3 and 4 represent the velocity field for different parameters affecting the flow field.

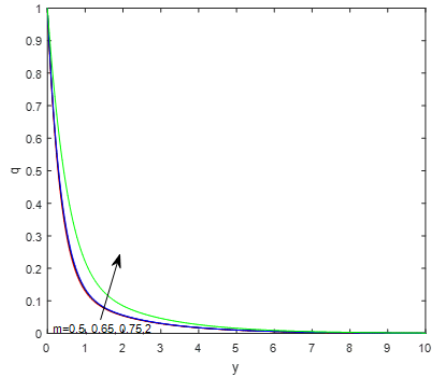

(a)

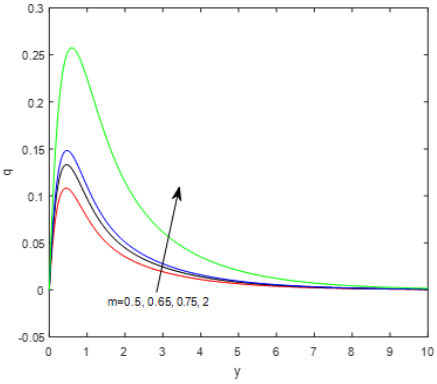

(b)

Figure 2. Effect of Hall current (m) on velocity profile (q) in (a) primary and (b) secondary flow

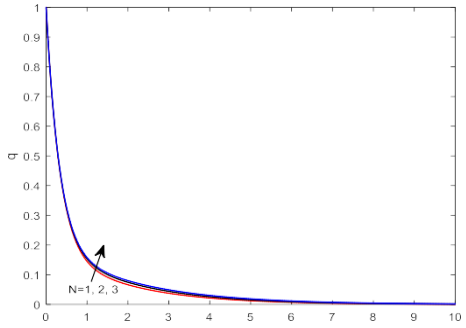

(a)

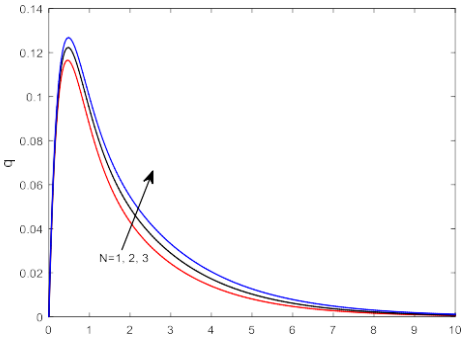

(b)

Figure 2. Effects of thermal radiation (N) on velocity profile (q) in (a) primary and (b) secondary flow

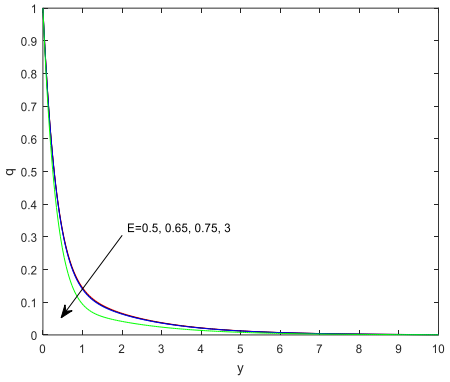

(a)

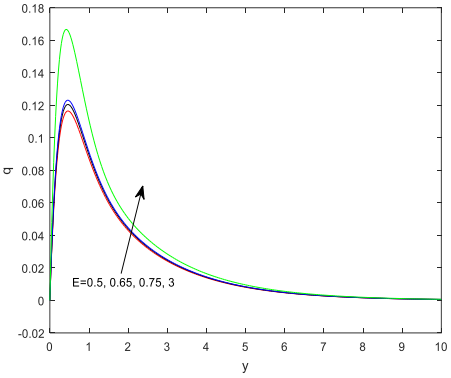

(b)

Figure 4. Effects of E on velocity profile (q) in (a) primary and (b) secondary flow

Figure 2 represents velocity profiles for Hall current (m). Due to boundary layer thickness, velocity profile (q) rises for rising value of the Hall current (m). Also, we know that electric field and magnetic strength of the magnetic field are proportional to the Hall current (m). Hence, rise in Hall current accelerates both primary and secondary velocity profiles (q).

The effect of thermal radiation (N) on the velocity profiles (q) is presented in Figure 3. It is noted that the N decelerates the buoyancy force, minimizing the boundary layer thickness. Therefore, velocity profile (q) accelerates with N. Physically the bond holding the components of the fluid particles is easily broken, when there is rise in the amount of heat generated through the N. Hence, we conclude that the radiation should be minimized to have faster rate of cooling. Also, we know that ambient temperature (T'_∞) is proportional to the radiation parameter (N) and the ambient temperature helps in cooling the fluid. Hence, rise in N accelerates velocity profiles (q) in both primary and secondary flow directions.

The effect of rotation parameter (E) in velocity profile (q) is depicted in Figure 4. Due to viscosity, rise in rotation parameter (E) decelerates the velocity profile (q) in primary flow direction. Also, due to characteristic velocity, rise in rotation parameter (E) accelerates the velocity profile (q) in secondary flow direction.

5.2 Induced magnetic field (i.m.f)

Figure 6 depicts the impact of Hall current (m) on i.m.f (h). Since electric field and magnetic strength of the magnetic field are proportional to the Hall current (m), an increase in Hall current contributes to both primary and secondary induced magnetic fields (h).

The effect of thermal radiation (N) is plotted in Figure 7. The rise in thermal radiation decelerates the primary i.m.f of the flow because thermal conductivity of the fluid and permeability of the porous medium are inversely proportional to the thermal radiation (N). Also, we note that ambient temperature (T'_∞) is proportional to the radiation parameter (N) and ambient temperature helps in cooling the fluid. Hence, rise in N accelerates secondary i.m.f of the flow.

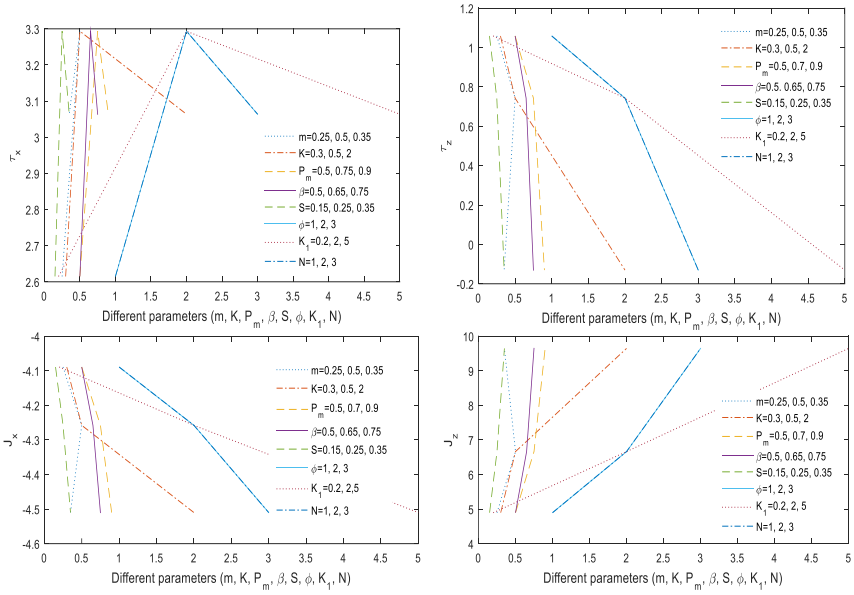

Figure 5. Effects of pertinent parameters on skin friction (τ_x, τ_z) and current density (J_x, J_z)

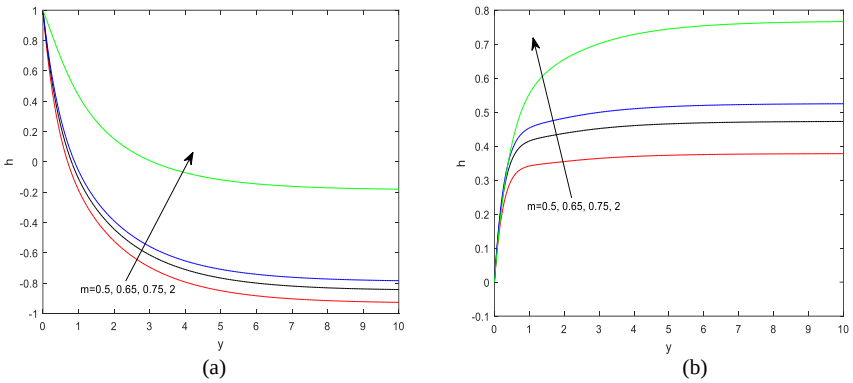

Figure 6. Effects of Hall current (m) on i.m.f. (h) in (a) primary and (b) secondary flow

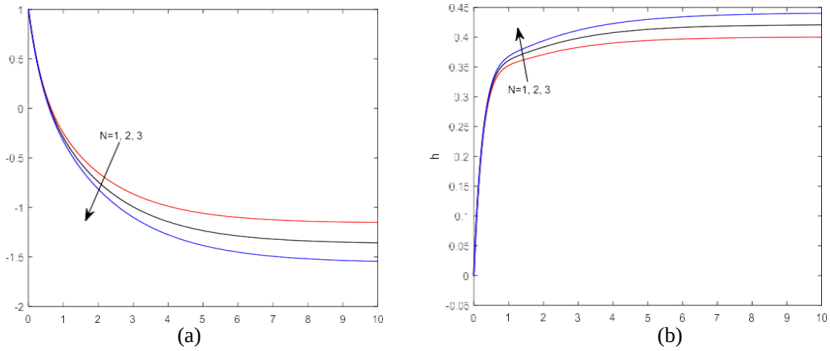

Figure 7. Effects of thermal radiation (N) on i.m.f. (h) in (a) primary and (b) secondary flow

5.3 Temperature and concentration

In Figure 8, it is seen that the N reduces the thermal buoyancy force, minimizing the thermal boundary layer thickness. Therefore, temperature (T) rises with rise in N. Physically the bond holding the components of the fluid particles is easily broken, when there is rise in the amount of heat generated through the N. Hence, it is seen that the radiation should be minimized to have a faster rate of cooling. Also, we know that ambient temperature (T'_∞) is proportional to the radiation parameter (N). Hence, rise in N contributes to concentration (C) in both primary and secondary flow.

In Figure 10, Schmidt number (S_c) is the ratio of the viscosity to the diffusion of mass. Due to the diffusion of mass, concentration (C) decreases with the rise in Schmidt number (S_c).

5.4 Quantities of physical interest

Figures 5 and 9, respectively, reflect the variations in Nusselt number (Nu), Sherwood number (Sh), current density (J) and skin friction (τ) at m.v.s corresponding to different flow inducing parameters.

A rise in Nusselt number (Nu) and Sherwood number (Sh) is noticed with rise in suction parameter (S), heat source parameter (ϕ), chemical reaction parameter (K_1), and thermal radiation (N).

Current density (J) at m.v.s in primary flow direction shows decreasing tendency with rising Hall current (m), magnetic Prandtl number (P_m), viscoelastic parameter (β), suction parameter (S), heat source parameter (ϕ), permeability parameter (K), chemical reaction parameter (K_1), and thermal radiation (N).

Hall current (m), magnetic Prandtl number (P_m), viscoelastic parameter (β), suction parameter (S), chemical reaction parameter (K_1), permeability parameter (K), heat source parameter (ϕ) and thermal radiation (N) have promoting effect on current density (J) at m.v.s in secondary flow direction.

In the main flow direction, skin friction (τ) increases with the Hall current (m). Skin friction (τ) first increases to its maximum, then decreases with an increase in magnetic Prandtl number (P_m), suction parameter (S), chemical reaction parameter (K_1), viscoelastic parameter (β), heat source parameter (ϕ) permeability parameter (K) and thermal radiation (N) at m.v.s in the primary flow direction.

In the secondary flow direction, skin friction (τ) at m.v.s decreases with Hall current (m), magnetic Prandtl number (P_m), suction parameter (S), chemical reaction parameter (K_1), viscoelastic parameter (β), heat source parameter (ϕ), permeability parameter (K), and thermal radiation (N).

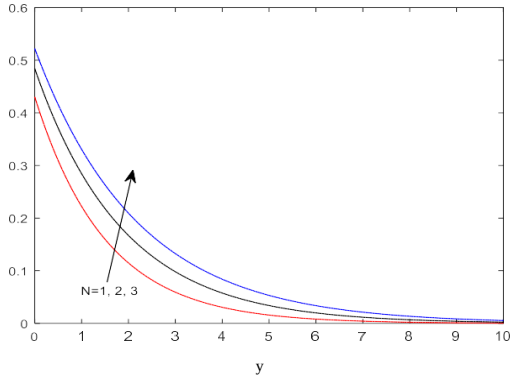

Figure 8. Thermal distributions by thermal radiation (N)

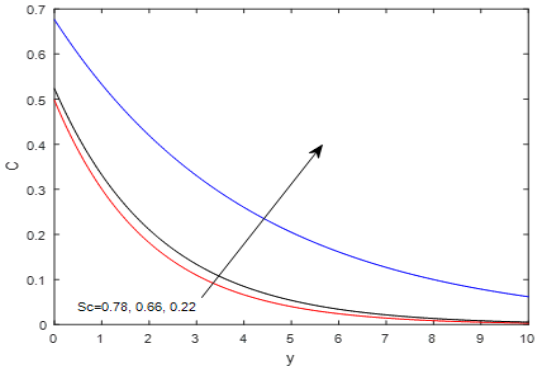

Figure 10. Effects on concentration (C) by Schmidt number (Sc)

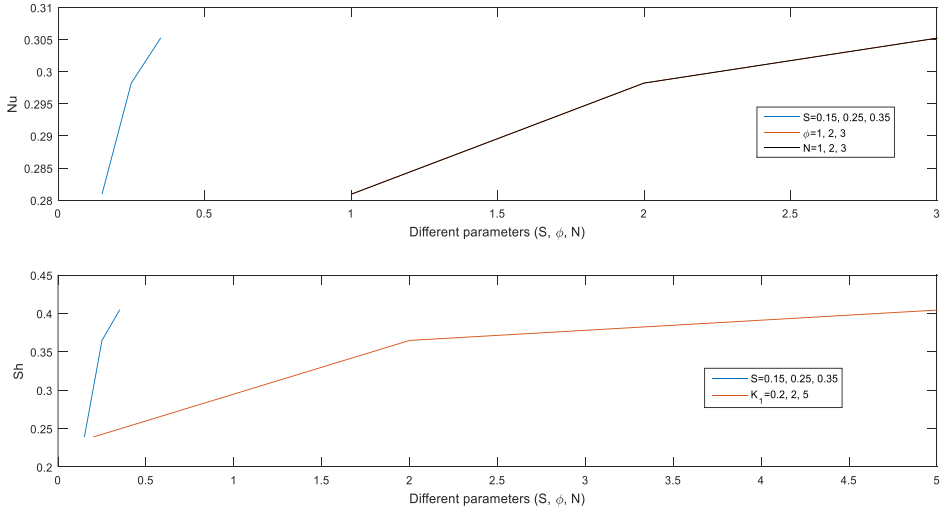

Figure 9. Effects of pertinent parameters on Nusselt number (Nu) and Sherwood number (Sh)

Table 1. Nu and Sh at m.v.s

S	Φ	Singh *et al*. (2020) Nu	N	Present work Nu	K_1	Singh *et al*. (2020) Sh	Present work Sh
0.15	1	0.3245	1	0.2809	0.2	0.2390	0.2390
0.25	1	0.3293	1	0.2847	0.2	0.2511	0.2511
0.35	1	0.3341	1	0.2884	0.2	0.2629	0.2629
0.25	2	0.3628	1	0.3232	0.2	0.2511	0.2511
0.25	3	0.3808	1	0.3446	0.2	0.2511	0.2511
0.25	1	0.3293	2	0.2578	2	0.3649	0.3649
0.25	1	0.3293	3	0.2388	5	0.4029	0.4029

Table 2. J and τ at m.v.s

m	K	P_m	β	S	Φ	K_1	N	$-J_x$	$-J_z$	$-\tau_x$	τ_z
0.5	0.3	0.75	0.5	0.25	1	0.2	1	-5.4165	7.6266	3.4181	1.1161
0.25								-3.1519	5.4915	3.6334	0.6501
0.35								-4.2118	6.5595	3.5627	0.8499
	0.5							-5.4102	7.2024	3.2068	1.2125
	2							-5.4089	6.7546	2.9465	1.3405
		0.5						-3.5098	4.6222	2.6192	1.0016
		0.9						-6.5821	9.5720	3.8293	1.1640
			0.65					-5.4170	8.4129	3.3555	0.9562
			0.75					-5.4173	8.9371	3.2712	0.8054
				0.15				-5.1916	6.5124	3.1628	1.1509
				0.35				-5.6186	8.7279	3.5726	0.9610
					2			-5.3545	7.6162	3.4692	1.0739
					3			-5.3301	7.6193	3.5041	1.0539
						2		-5.2841	7.5840	3.6037	0.9610
						5		-5.3366	7.6071	3.6950	0.9275
							2	-5.4779	7.6512	3.3955	1.1513
							3	-5.5336	7.6805	3.3884	1.1799

5.5 Numerical validation of results

To verify the accuracy of our results, we have compared the effects of Hall current (m) on velocity profile (q) in primary flow direction and it was found that our investigation is in good agreement with Singh *et al.* (2020) when thermal radiation (N) is 0.

6. Conclusions

In this paper, we have modeled radiation effects on MHD mixed convection flow over m.v.s with hall current and i.m.f, and performed mathematical analysis. Various flow parameters were mathematically represented. Some important observations are as follows:

- Thermal radiation increases velocities in both primary and secondary flow directions.
- Thermal radiation decreases i.m.f in primary flow direction but the reverse trend is seen in the secondary flow direction.
- Temperature profiles rise with rise in thermal radiation (N).
- Nusselt number decreases with rise in thermal radiation (N).
- Skin friction reduces in the primary flow direction with rise in thermal radiation (N) but s reverse effect is seen in the secondary flow direction.
- Current density rises in the secondary flow direction with rise in thermal radiation (N) while a reverse effect is seen in the primary flow direction.

Nomenclature

B_i	Biot number
C	non-dimensional species concentration
C'	species concentration)mol/m^3(
C_p	specific heat at constant pressure)J/Kg·K(
C'_w	concentration near wall)mol/m^3(
C'_∞	ambient concentration)mol/m^3(
D_m	chemical molecular diffusivity
E	rotation parameter
F_i	solutal Biot number
g	acceleration due to gravity)m/s^2(
G_C	solutal Grashof number
G_T	thermal Grashof number
B_i	Biot number
C	non-dimensional species concentration
C'	species concentration)mol/m^3(
C_p	specific heat at constant pressure)J/Kg·K(
C'_w	concentration near wall)mol/m^3(
C'_∞	ambient concentration)mol/m^3(
D_m	chemical molecular diffusivity
E	rotation parameter
F_i	solutal Biot number
g	acceleration due to gravity)m/s^2(

G_C	solutal Grashof number
G_T	Thermal Grashof number
H_0	constant magnetic field
h_0	applied magnetic field
h_c	coefficient of convective mass transfer
h_f	coefficient of convective heat transfer
(h_x, h_y, h_z)	dimensionless induced magnetic field components
$)h'_x, h'_y, h'_z($	induced magnetic field components
(J_x, J_y, J_z)	dimensionless current density components
k	thermal conductivity of the fluid)W/m·K(
K	permeability parameter
k'	permeability of the porous medium $)m^2($
K'	chemical reaction coefficient
K_1	chemical reaction parameter
m	Hall current parameter
M	magnetic parameter
M_0	constant
P_m	magnetic Prandtl number
P_r	Prandtl number
S	suction parameter
S^*	heat source coefficient
S_c	Schmidt number
T	non-dimensional fluid temperature
T'	fluid temperature)K(
T'_w	wall temperature)K(
T'_∞	ambient temperature)K(
(u, v, w)	dimensionless velocity components
(u', v', w')	velocity components along)m/s(
U_0	characteristic velocity)m/s(
v_0	transpiration velocity)m/s(
(x', y', z')	Cartesian coordinates
N	radiation number
q_r	radiative heat flux $)W/m^2($
k'	mean absorption coefficient

Greek symbols

β	viscoelastic parameter
β'	viscoelastic coefficient
μ_e	magnetic permittivity
υ_e	effective coefficient of viscosity $)m^2/s($
υ_f	coefficient of viscosity $)m^2/s($
υ_m	magnetic viscosity
ρ	fluid density $)kg/m^3($
σ	electrical conductivity)s/m(
(τ_x, τ_y, τ_z)	dimensionless skin friction components
ϕ	heat source parameter
β_T	volumetric coefficient of thermal expansion
β_C	volumetric coefficient of concentration expansion
σ'	Stefan- Boltzmann constant

Acknowledgements

We are thankful to Department of Science and Technology, Government of India, New Delhi, for providing fund for our research work in terms of Inspire Fellowship.

References

Baitharu, A., Sahoo, S., & Dash, G. (2020a). Heat and mass transfer effect on a radiative second grade MHD flow in a porous medium over a stretching sheet. *Journal of Naval Architecture and Marine Engineering*, *17*(1), 51–66.

Baitharu, A., Sahoo, S., & Dash, G. (2021a). Effect of joule heating on steady MHD convective micropolar fluid over a stretching/shrinking sheet with slip flow model. *Journal of Naval Architecture and Marine Engineering*, *18*(2), 175–186.

Baitharu, A. P., Sahoo, S., & Dash, G. (2021b). Convective boundary layer flow and heat transfer of polar fluid in vertical concentric annuli with thermal slip. *International Journal of Ambient Energy*, 1–9.

Baitharu, A. P., Sahoo, S., & Dash, G. C. (2020b). Numerical approach to non-Darcy mixed convective flow of non-Newtonian fluid on a vertical surface with varying surface temperature and heat source. *Karbala International Journal of Modern Science*, *6*(3), 12.

Chaudhary, R., Sharma, B. K., & Jha, A. K. (2006). Radiation effect with simultaneous thermal and mass diffusion in MHD mixed convection flow from a vertical surface with Ohmic heating. *Romanian Journal of physics*, *51*(7/8), 715.

Hayat, T., Abbas, Z., &Sajid, M. (2009). MHD stagnation-point flow of an upper-convected Maxwell fluid over a stretching surface. *Chaos, Solitons and Fractals*, *39*(2), 840–848.

Hayat, T., Ullah, I., Muhammad, T., &Alsaedi, A. (2017). Radiative three dimensional flow with Soret and Dufour effects. *International Journal of Mechanical Sciences*, *133*, 829–837.

Iqbal, M. S., Malik, F., Mustafa, I., Ghaffari, A., Riaz, A., & Nisar, K. S. (2020). Impact of induced magnetic field on thermal enhancement in gravity driven Fe_3O_4 ferrofluid flow through vertical non-isothermal surface. *Results in Physics*, *19*, 103472.

Iqbal, Z., Maraj, E. N., Azhar, E., & Mehmood, Z. (2017). Framing the performance of induced magnetic field and Entropy generation on Cu and TiO_2 nanoparticles by using Keller Box Scheme. *Advanced Powder Technology*, *28*(9), 2332-2345.

Jamil, M., Khan, A. N., & Shahid, N. (2013). Fractional magnetohydrodynamicsOldroyd-B fluid over an oscillating plate. *Thermal Science*, *17* (4), 997–1011.

Khemissat, B., Bouaziz, A. M., & Bouaziz, M. (2022). Thermophoretic andsuction/blowing effects on MHD mixed convection flow over an inclinedplate combined with heat generation, chemical reaction and radiation. *Defect and Diffusion Forum*, *415*, 3–20.

Koshiba, Y., Matsushita, T., & Ishikawa, M. (2002). Influence of induced magnetic field on large-scale pulsed MHD generator. *Proceeding of the 33rd Plasmadynamics and Lasers Conference*.

Krishna, M. V. (2021a). Hall and ion slip effects on radiative MHD rotating flow of Jeffreys fluid past an infinite vertical flat porous surface with rampedwall velocity and temperature. *International Communications in Heat and Mass Transfer*, *126*, 105399.

Krishna, M. V. (2021b). Radiation-absorption, chemical reaction, hall andion slip impacts on magnetohydrodynamic free convective flow over semi- infinite moving absorbent surface. *Chinese Journal of Chemical Engineering*, *34*, 40–52.

Krishna, M. V., & Chamkha, A. J. (2020). Hall and ion slip effects on unsteady MHD convective rotating flow of nanofluids—application in biomedical engineering. *Journal of the Egyptian Mathematical Society*, *28*(1), 1–15.

Meher, R., & Patel, N. (2020). Numerical study of magnetohydrodynamics Jeffery–Hamel flow with cu-water nanofluid between two rectangular smooth walls with transverse magnetic field. *International Journal of Computational Materials Science and Engineering*, *9*(2), 2050010.

Meher, R., & Patel, N. D. (2019). Analytical investigation of MHD Jeffery– Hamel flow problem with heat transfer by differential transform method. *SN Applied Sciences*, *1*(7), 1–12.

Osalusi, E., Side, J., Harris, R., & Clark, P. (2008). The effect of combinedviscous dissipation and joule heating on unsteady mixed convection MHD flow on a rotating cone in a rotating fluid with variable properties in thepresence of hall and ion-slip currents. *International Communications in Heat and Mass Transfer*, *35*(4), 413–429.

Panda, J., Dash, N., & Dash, G. (2012). Heat and mass transfer on MHD flow through porous media over an accelerating surface in the presenceof suction and blowing. *Journal of Engineering Thermophysics*, *21* (2), 119–130.

Pandya, N., & Quraishi, M. S. (2018). Effect of chemical reaction and rotationon MHD unsteady flow past an inclined oscillating infinite porous plateembedded in porous medium for heat generation/absorption with masstransfer and variable temperature. *International Journal of Mathematics and its Application*, 6(1-E), 965-975

Panigrahi, L., Kumar, D., & Panda, J. (2021). Impact of chemical reaction, hall current, and radiation on MHD flow between vertical walls. *Journalof Engineering Thermophysics*, *30*(1), 122–144.

Sahoo, S., Rout, P. K., & Dash, G. C. (2022). Radiation effect on MHD flow through porous medium past a vertical plate with time dependent surface temperature and concentration. *Songklanakarin Journal of Science and Technology*, *44*(3), 698 – 707, doi:10.14456/sjst-psu.2022.95

Sahoo, S., Panda, J., & Dash, G. (2013). The MHD mixed convection stagnationpoint flow and heat transfer in a porous medium. *Proceedings of the National Academy of Sciences, India Section A: Physical Sciences*, *83*(4), 371–381.

Singh, J. K., Shanker Seth, G., Vishwanath, S., & Rohidas, P. (2020). Steady MHD mixed convection flow of a viscoelastic fluid over a magnetized convectively heated vertical surface with hall current and induced magnetic field effects. *Heat Transfer*, *49*(8), 4370-4393.

Veera Krishna, M. (2020). Hall and ion slip effects on MHD free convectiverotating flow bounded by the semi-infinite vertical porous surface. *Heat Transfer*, *49*(4), 1920–1938.

VeeraKrishna, M., Subba Reddy, G., & Chamkha, A. (2018). Hall effectson unsteady MHD oscillatory free convective flow of second grade fluidthrough porous medium between two vertical plates. *Physics of Fluids*, *30*(2), 023106.

Verma, L., & Meher, R. (2022). Effect of heat transfer on Jeffery–Hamel Cu/Ag– water nanofluid flow with uncertain volume fraction using the double parametric fuzzy homotopy analysis method. *The European Physical Journal Plus*, *137*(3), 1–20.